



Article

# Evaluation of Grid-Based Rainfall Products and Water Balances over the Mekong River Basin

Kha Dang Dinh <sup>1,\*</sup>, Tran Ngoc Anh <sup>1,2</sup>, Nhu Y Nguyen <sup>1</sup>, Du Duong Bui <sup>3</sup> and Raghavan Srinivasan <sup>4</sup>

<sup>1</sup> Department of Hydrology and Water Resources, University of Science, Vietnam National University, Hanoi, 334 Nguyen Trai, Thanh Xuan, Hanoi 100000, Vietnam; tranngocanh@hus.edu.vn (T.N.A.); nguyennhu@hus.edu.vn (N.Y.N.)

<sup>2</sup> Center for Environmental Fluid Dynamics, University of Science, Vietnam National University, Hanoi, 334 Nguyen Trai, Thanh Xuan, Hanoi 100000, Vietnam

<sup>3</sup> National Center for Water Resources Planning and Investigation, Ministry of Natural Resources and Environment of Vietnam, 10 Tôn Thất Thuyết, Hà Nội 100000, Vietnam; bdduong@monre.gov.vn

<sup>4</sup> Departments of Ecosystem Sciences and Management and Biological and Agricultural Engineering at Texas A&M University, Texas, TX 77843, USA; r-srinivasan@tamu.edu

\* Correspondence: dangdinhkha@hus.edu.vn

Received: 28 April 2020; Accepted: 3 June 2020; Published: 8 June 2020



**Abstract:** Gridded precipitation products (GPPs) with wide spatial coverage and easy accessibility are well recognized as a supplement to ground-based observations for various hydrological applications. The error properties of satellite rainfall products vary as a function of rainfall intensity, climate region, altitude, and land surface conditions—all factors that must be addressed prior to any application. Therefore, this study aims to evaluate four commonly used GPPs: the Climate Prediction Center (CPC) Unified Gauge-Based Analysis of Global Daily Precipitation, the Climate Prediction Center Morphing (CMORPH) technique, the Tropical Rainfall Measuring Mission (TRMM) 3B42, and the Global Satellite Mapping of Precipitation (GSMaP), using data collected in the period 1998–2006 at different spatial and temporal scales. Furthermore, this study investigates the hydrological performance of these products against the 175 rain gauges placed across the whole Mekong River Basin (MRB) using a set of statistical indicators, along with the Soil and Water Assessment Tool (SWAT) model. The results from the analysis indicate that TRMM has the best performance at the annual, seasonal, and monthly scales, but at the daily scale, CPC and GSMaP are revealed to be the more accurate option for the Upper MRB. The hydrological evaluation results at the daily scale further suggest that the TRMM is the more accurate option for hydrological performance in the Lower MRB, and CPC shows the best performance in the Upper MRB. Our study is the first attempt to use distinct suggested GPPs for each individual sub-region to evaluate the water balance components in order to provide better references for the assessment and management of basin water resources in data-scarce regions, suggesting strong capabilities for utilizing publicly available GPPs in hydrological applications.

**Keywords:** gridded precipitation products; GSMaP; SWAT; CMORPH; TRMM; CPC; Mekong River Basin; water balance components

## 1. Introduction

It is well recognized in the literature that precipitation is one of the key factors in hydrological application practices [1–3]. Existing precipitation products generally include gauge observations, estimates inferred from satellite imagery, and outputs from various numerical models [4]. The strengths and weaknesses of different kinds of precipitation data vary greatly. While the data quality of in

situ rain gauges is the most reliable, their spatial distribution is often sparse and uneven, as data availability in complex terrain regions is limited [5–7]. The quality of ground-based weather radars is also unreliable, as it can be affected by signal distortion [8–10]. Gridded precipitation products (GPPs; i.e., re-analysis, satellite, and model-based products) have high spatial and temporal resolutions, but they also have a high level of uncertainty, affected by retrieval algorithms, data sources [11], and gauge adjustment procedures [12–14]. Precipitation itself strongly varies in relation to different climate properties, altitudes, and surface conditions [15]. These strengths and weaknesses and the variability of precipitation thus affect hydrological simulation and water balance components.

As a result, the selection of the best precipitation input for a hydrological model is basin-specific; especially in the case of large, complex basins stretching across different climatic zones and topographies, as with the Mekong River Basin (MRB) [16,17]. Therefore, selection of the correct hydrological model [18] is crucial to ensure a high-accuracy assessment of water balance components, which constitutes an important issue for analyzing and developing strategies for current and future problems in sustainable water resource management. In a large number of hydrological models, the Soil and Water Assessment Tool (SWAT) [19] is widely used with little direct calibration being required to obtain good hydrologic predictions [20], and this method is helpful in identifying and calculating the components of water balance.

Owing to its wide coverage and enhanced tempo-spatial resolutions, remote sensing contributes valuably to the monitoring of hydrological variables and hydrological predictions regionally and globally, particularly in areas with a limited capability of surface-based observations [2,21,22]. In typical satellite products, precipitation products are usually generated based on thermal infrared, passive microwave, and radar data, and then calibrated by using ground observations of rainfall to obtain better estimations [7]. Over the last few decades, multiple satellite projects have been launched. Various global GPPs are available online, such as the Climate Prediction Center (CPC) Unified Gauge-Based Analysis of Global Daily Precipitation datasets provided by National Oceanic and Atmospheric Administration (NOAA) [23], the Tropical Rainfall Measuring Mission (TRMM) precipitation data [24], the Climate Prediction Center Morphing (CMORPH) product [25], and the Global Satellite Mapping of Precipitation (GSMaP) product [26]. These GPPs have a large spatial and frequent temporal coverage and provide potential alternative data sources for hydrological studies and water resource management, especially in data-sparse and ungauged regions.

At present, there is a demand for fuller awareness of the strengths and weaknesses of publicly available GPPs and rain gauge observations across different regions for more in-depth hydrological studies and improved water resources management. Over the Lower Mekong River Basin (from the place where the Mekong River leaves Yunnan province (China) and enters the Golden Triangle tripoint), Mohammed et al. [27] suggested that streamflow simulation by forcing TRMM data is able to capture the variability of observation, and is even better than using in situ precipitation data. In other research, Wang et al. [28] also confirmed that TRMM-forcing simulation performed well compared to observations for the regions with sparsely-distributed stations. Several studies have quantitatively assessed various precipitation products over the MRB [27,28]. Analysing its potential in water balance assessment has not, however, received much attention.

As a trans-boundary river basin, the economies and societies along the Mekong River have different priorities for water resources management. Changing the global climate and the trans-boundary nature of the river adds complexity to water-related issues in the catchment [28–31].

Therefore, with the aim to further analyze which GPP is the most appropriate for water balance component analysis under the complex features of the MRB, this study: (1) evaluates and compares the performance of four GPPs (CPC, TRMM 3B42, GSMaP\_Gauge, CMORPH—from here, the term GPPs only refers to the four selected GPPs) on variant time and spatial scales to characterize the precipitation patterns over the whole MRB; and (2) investigates the water balance components across different regions using these products as inputs for the SWAT model.

## 2. Materials and Methods

### 2.1. Study Area

The Mekong River is the largest river in South East Asia, flowing 4909 km with a total basin area of 795,000 km<sup>2</sup> and an average discharge of 14,500 m<sup>3</sup>/s, distributed unevenly across six countries: China (21%), Myanmar (3%), Lao People's Democratic Republic (Lao PDR) (25%), Thailand (23%), Cambodia (20%), and Vietnam (8%) [32]. The MRB ranges from temperate to tropical monsoon climate. The Upper Basin in China (known as Lancang) is glaciated, starting in the Tibetan Plateau (Figure 1). The Lower Mekong Basin starts from Yunnan province downstream (China) and flows through the Golden Triangle tripoint to the South China Sea (known as the Lower Mekong Basin), and is classified as tropical monsoon [32]. The watershed has a complex topography, with the elevations in the basin ranging from above 6000 m in the Tibetan Plateau to less than a meter (0.3–0.7 m) above sea level in the downstream river delta, and with deep-cut valleys in the high mountains [32,33].

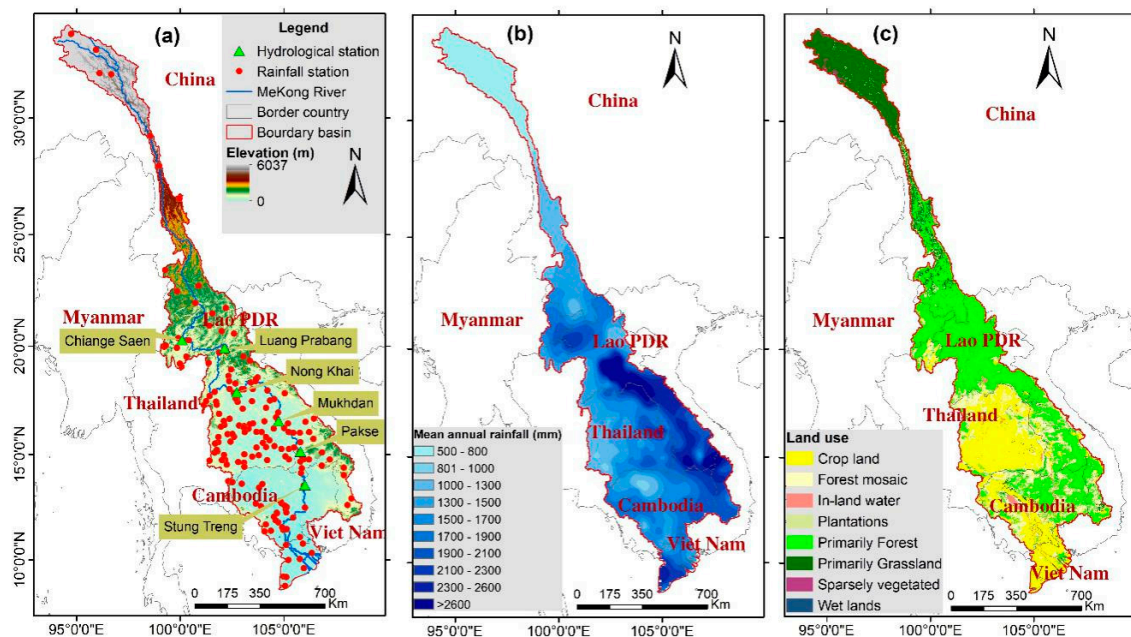


**Figure 1.** Map of the Mekong River Basin: (a) Rainfall and the hydrological station network; (b) mean annual rainfall; (c) land use map (Data source: MRC [33]).

Overall, acrisols are the most common type of soil in the MRB, comprising around 65% of the total land area. Acrisols are common to humid tropical climates, and are a weathered-type, clay-rich, and low-nutrient soil, posing limitations for agriculture and thus being commonly forested. Lithosols are the second most common type of soil in the MRB, found in the upper, steep mountainous areas and common to highly erodible grassland [32,33].

Land use can be broadly divided into three major components: agriculture (32%), forested land (39%), and grassland (9%). The majority of the MRB is covered by forest, mainly located in Lao PDR and Cambodia. Grassland dominates the upper basin and agricultural land dominates the low-lying plains of the Chi–Mun Basin in northeast Thailand, the Vientiane plain in Lao PDR, the Tonle Sap Basin in Cambodia, and the delta in southern Vietnam (Figure 1) [32,33].

As can be seen from the spatial contrasts in rainfall, much of the monsoonal rain is captured in the Northern and Eastern Highlands, creating dry conditions across the Korat Plateau. The mean annual rainfall is 1300 mm, more than 70% of which falls in the summer season. The dry season lasts from December to May, and evapotranspiration is high during this time. The river flow has a distinct seasonal pattern, with high flows from June to November that account for 80%–90% of the total annual

flow [34]. The annual flood season is especially important in the Lower Mekong Basin, where it has shaped the environment and its inhabitants.

## 2.2. Materials

### 2.2.1. Rainfall Datasets

The ground rainfall data from 1998 to 2006 used in this study were obtained from the Mekong River Commission (MRC) and the China Meteorological Administration (CMA). Data were collected from a series of 175 rain gauges over the study area (Figure 1a). The GPPs included CPC, TRMM, and CMORPH over the period of 1998–2006, and GSMaP over the period of 2000–2006, which were selected for evaluation in the MRB (Table 1). For global land areas, the CPC data used in the current global/regional gridded datasets were mainly retrieved from the World Meteorological Organization (WMO) Global Telecommunication System (GTS) based on the optimal interpolation (OI) method [35] on a  $0.5 \times 0.5^\circ$  grid. It should be noted that within the MRB, the number of GTS gauges operating over the period of 1998–2006 was relatively low—30 gauges (1998–2002) and 40 gauges (2002–2006)—compared to 175 rain gauges from the MRC and the CMA. Moreover, these satellite precipitation products (GSMaP, TRMM, and CMORPH) were calibrated with the CPC and the Global Precipitation Climatology Center (GPCC) [36] products to obtain higher accuracy.

**Table 1.** The information datasets used in this study.

Data type	Products	Spatial Resolution	Temporal Resolution	Sources/References
Meteorological data	Temperature, solar radiation, wind speed, relative humidity, potential evapotranspiration	$0.25^\circ \times 0.25^\circ$	Daily 1998–2006	The National Centers for Environmental Prediction (NCEP)
	Rain gauge observations	Point (175 rain gauges)	Daily 1998–2006	The Mekong River Commission (MRC) and the China Meteorological Administration (CMA)
Rainfall	Climate Prediction Center (CPC) Gauge-based Analysis of Global Daily Precipitation	$0.5^\circ \times 0.5^\circ$	Daily 1998–2006	[23]
	Global Satellite Mapping of Precipitation (GSMaP) Version 6	$0.1^\circ \times 0.1^\circ$	Daily March 2000 to 2006	[26]
	Climate Prediction Center Morphing (CMORPH) Version 1.0	$0.25^\circ \times 0.25^\circ$	Daily 1998–2006	[25]
	Tropical Rainfall Measuring Mission (TRMM) Version 7, 3B42	$0.25^\circ \times 0.25^\circ$	Daily 1998–2006	[24]
Geography	Digital Elevation Model (DEM)	$90 \times 90$ m	2005	[37]
	Land use	$1 \times 1$ km	2005	[33]
	Soil	$10 \times 10$ km	2005	[38]
Hydrology	Discharge	Point (6 hydrological gauges)	Daily 1998–2006	[33]

### 2.2.2. Other Data

The meteorological data were obtained from The National Centers for Environmental Prediction (NCEP) over the same period as the rainfall data—1998 to 2006. The other required data, including that of the Digital Elevation Model (DEM), the MRB land use maps, and the soil, were collected from USGS-HydroSHEDS [37], the MRC [33], and the Food and Agriculture Organization [38].

### 2.2.3. Discharge Data

The discharge observations from six gauges along the main stream of the Mekong River provided by the MRC were used for the calibration of the SWAT model and the evaluation of the precipitation products—i.e., Chiange Saen, Luang Prabang, Nong Khai, Mukhdan, Pakse, and Stung Treng. The catchment area and location are given in Table 2 and Figure 1.

**Table 2.** The hydrological stations used for the Soil and Water Assessment Tool (SWAT) model’s calibration.

Station	Longitude (Degree)	Latitude (Degree)	Area (km <sup>2</sup> )	% of Whole Basin
Chiange Saen	100.08	20.27	189,000	23.8
Luang Prabang	102.14	19.89	268,000	33.7
Nong Khai	102.72	17.88	302,000	38.0
Mukhdan	104.74	16.54	391,000	49.2
Pakse	105.80	15.12	545,000	68.6
Stung Treng	106.02	13.55	635,000	79.9
Total			795,000	100

Note: Data Source: MRC [33].

## 3. Methods

Owing to the two specific objectives of this study, the following two methods were used:

- (1) Statistical evaluation metrics were employed for evaluating the performance of the GPPs compared with the “actual” precipitation patterns derived from the gauge-based rainfall observations.
- (2) The SWAT model was used to investigate how accurately the GPPs are able to model hydrologic processes, while statistical metrics (i.e., the Nash–Sutcliffe efficiency coefficient (NSE), percent bias (PBIAS), and coefficient of determination ( $R^2$ )) were used to evaluate the model’s performance, followed by the SWAT model to analyze the water balance components in each sub-region of the MRB.

### 3.1. Statistical Evaluation of GPPs against Gauge Observations

In order to analyze the performance of GPPs in capturing precipitation, three types of indices were used:

- i. Four basic statistical indicators, including correlation coefficient (CC), standard error (SE), root-mean-squared deviation (RMSD), mean absolute error (MAE), and percentage bias (PBIAS), all computed at different temporal and spatial scales (Table 3).
- ii. Evaluation of the capability of the GPPs to detect rain and non-rain days, which plays an important role in hydrological applications [39]. Therefore, in this study, three indicators—including probability of detection (POD), critical success index (CSI), and false alarm ratio (FAR)—were employed (Table 3). POD is typically used to describe the proportions of rainy days that are correctly detected by GPPs to the total observations [40]; CSI reflects the overall proportion of rainfall events that are correctly detected by GPPs; and FAR describes the proportions of rainy days that are not recorded by the rain gauges to the total observations.
- iii. Evaluation of the variability and distributions of the GPPs following different rainfall intensities by classifying five daily rainfall thresholds: (1) rain  $\leq$  0.1 mm (no rain); (2) 0.1 < rain  $\leq$  1 mm (little rain); (3) 1 < rain  $\leq$  20 mm (light rain); (4) 20 < rain  $\leq$  50 mm (moderate rain); (5) rain > 50 mm (heavy rain) [41].



**Table 3.** The statistical metrics and their corresponding equations used for evaluating the overall performance of satellite precipitation products.

Statistical Metric	Unit	Equation	Optimal Value
Correlation coefficient (CC)	-	$CC = \frac{\sum_{i=1}^n (O_i - \bar{O})(P_i - \bar{P})}{\sqrt{\sum_{i=1}^n (O_i - \bar{O})^2} \sqrt{\sum_{i=1}^n (P_i - \bar{P})^2}}$	1
Standard error (SE)	-	$SE = \frac{\sigma}{\sqrt{n}}$	
Root-mean-squared deviation (RMSD)	mm	$RMSD = \sqrt{\frac{1}{n} \sum_{i=1}^n (O_i - P_i)^2}$	0
Mean absolute error (MAE)	mm	$MAE = \frac{1}{n} \sum_{i=1}^n  O_i - P_i $	0
Percent bias (PBIAS)	%	$PBIAS = \frac{\sum_{i=1}^n (P_i - O_i)}{\sum_{i=1}^n O_i} \times 100$	0
Nash–Sutcliffe efficiency coefficient (NSE)	-	$NSE = 1 - \frac{\sum_{i=1}^n (O_i - P_i)^2}{\sum_{i=1}^n (O_i - \bar{O})^2}$	1
Probability of detection (POD)	-	$POD = \frac{T}{T+M}$	1
False alarm ratio (FAR)	-	$FAR = \frac{F}{T+F}$	0
Critical success index (CSI)	-	$CSI = \frac{T}{T+M+F}$	0

Note: n, number of samples;  $O_i$ , observed precipitation (or observed streamflow);  $P_i$ , the precipitation estimates from the evaluated products (or simulated streamflow); T, the total number of the rainy days that the gridded precipitation products (GPPs) successfully detect rain; M, the number of days that the GPPs fail to detect the observed rain; F, the number of days that the GPPs fail to detect no-rain cases (unsuccessful no-rain detection);  $\sigma$ , standard deviation.

### 3.2. Modeling Method for Hydrological Evaluation of Daily Rainfall Series

#### 3.2.1. Model Setup

ArcSWAT 2012, interfacing in ArcGIS 10.2, was used to simulate the hydrological properties of the MRB. The sub-basins were delineated using the SWAT watershed analysis module (watershed delineator) based on the DEM  $90 \times 90$  m data and the stream network, resulting in 383 sub-basins in the MRB, with the average area of a sub-basin being around 2000 km<sup>2</sup>. The sub-basins were then further divided into hydrologic response units (HRUs)—consisting of homogeneous land use, management, topographical, and soil characteristics—by the HRU module in SWAT, using the land use, soil characteristics, slope, and stream network of 2005 (Table 1). In this way, we obtained 2850 HRUs for the MRB according to five slope classifications: 0%–2%, 2%–6%, 6%–15%, 15%–25%, and >25%. Then, the basin was divided into five elevation bands (0–500 m, 500–1000 m, 1000–1500 m, 1500–2000 m, and >2000 m) to improve model performance in the runoff simulation [11,39].

The precipitation data needed to be imported into SWAT in the form of point data. It should be noted that the rainfall data of the station closest to the centroid of each sub-basin were used, but the number of sub-basins was much smaller than the gridded precipitation data (383 sub-basins in the MRB compared to 1689 gridded points at  $0.25^\circ \times 0.25^\circ$  resolution). Therefore, the virtual precipitation station method proposed by Ruan et al. [42] was applied to estimate the precipitation for the sub-basins by taking the average value of all of the grids within the sub-basins from the GPPs. A total of 383 virtual precipitation stations were then created, and their estimated precipitation values were provided as inputs for the SWAT model.

#### 3.2.2. Model Calibration

The parameters and the default range recommended by previous studies [27,43–45] were first selected for sensitivity analysis and calibration in the current study. Then, one-at-a-time (OAT) in SWAT Calibration and Uncertainty Procedures (SWAT-CUP), each parameter was held constant, changing only one parameter at a time, to identify its effect on the model output or objective function. The results were used to fill out more sensitive parameters among the initial selection. The SWAT-CUP software package with the SUFI-2 algorithm was used for calibration, validation, and sensitivity analysis [45], because it is recognized as a robust tool for model calibration and validation [16,42,46]. The values of

the parameters were calibrated with four iterations, using 1500 model runs for each iteration, by the SUFI-2 method.

To evaluate model performance, the NSE [47] and the coefficient of determination ( $R^2$ ) were used. Uncertainties were quantified by two measures: P-factor and R-factor. P-factor is the percentage of observation points bracketed by 95% prediction uncertainty (95PPU) to measure the degree of uncertainty, and R-factor is the average width of the 95PPU band divided by the standard deviation of the observed values to reflect the strength of the uncertainty analysis, for which a P-factor above 0.70 and an R-factor of around 1 are considered satisfactory simulations [45].

## 4. Results and Discussion

### 4.1. Statistical Evaluation of GPPs

#### 4.1.1. Seasonal (Rainy/Dry) and Annual Comparison

The results from the analysis of the seasonal and annual variations of the precipitation of all of the GPPs and rain gauges at the grid scale for the period of 1998–2006 are shown in Figure 2. The results show an increasing trend in the precipitation from the northern part (upstream) to south-east part (downstream) of the MRB in all precipitation data for the dry and rainy seasons, as well as the entire year in general.

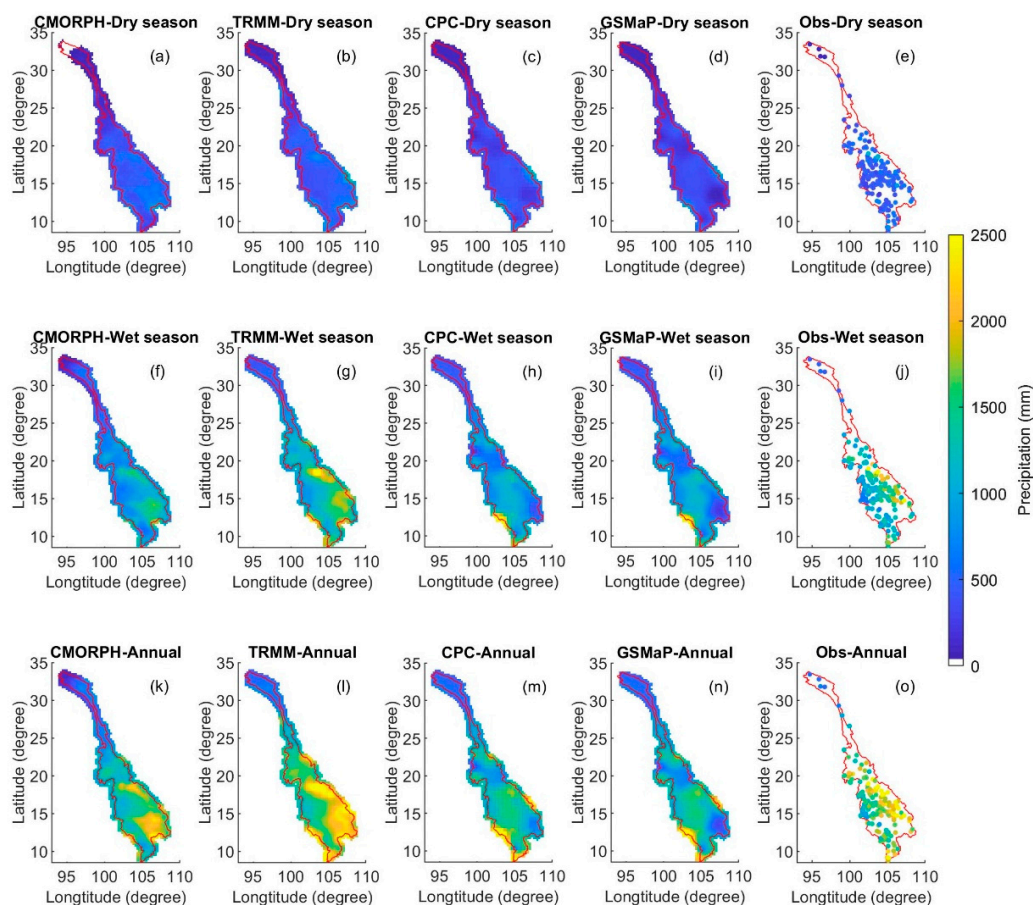


**Figure 2.** Average annual precipitation (mm/year) at a spatial resolution of  $0.25^\circ$  derived from the Climate Prediction Center Morphing (CMORPH), the Tropical Rainfall Measuring Mission (TRMM) 3B42, the Climate Prediction Center (CPC) Unified Gauge-Based Analysis of Global Daily Precipitation, and the Global Satellite Mapping of Precipitation (GSMaP): Observations for the dry season (a–e), the rainy season (f–j), and the entire year (k–o) over the Mekong River Basin during the period from 1998 to 2006.

Visual inspection of spatial distributions reveals that TRMM has the best agreement with the observation pattern (Figure 2b,g). The spatial distributions and precipitation amount of CPC and GSMaP are similar, but they are different to the observation pattern. Particularly, CPC and GSMaP show a distinct rainfall pattern with much lower precipitation over the northeast and mid-latitude regions (Figure 2c,d). This is possibly because the number of GTS gauges that provide data for CPC is insufficient to capture the precipitation pattern of these sub-areas. CMORPH reveals a relatively similar spatial distribution pattern as that of the TRMM 3B42 at the mid-latitude and low-latitude parts of the river basin, even though apparently lower precipitation amounts are observed. The spatial precipitation patterns in the upstream part of the basin (i.e., the northern part) for both seasons using CMORPH are very distinct from the observation pattern and the other evaluated GPPs—this product’s precipitation amount is extremely low compared to the others. The performances of the GPPs at the annual scale exhibit a similar pattern to the results at the seasonal scale.

It is clear that the spatial patterns of precipitation need to be considered when using these GPPs; TRMM 3B42 is able to capture the temporal (at both the seasonal and annual time scales) and spatial distribution patterns of precipitation better than the other evaluated GPPs over the MRB, and can be considered as a good alternative to rain gauges for hydrological research applications at these evaluated scales.

#### 4.1.2. Monthly Comparison

The monthly average precipitation time series in the basin for the GPPs during the period 1998–2006 were evaluated against the rain gauge data at different spatial scales (i.e., basin and pixel scales).

Relatively good agreements with the rain gauge data were observed in the CC indicator for all of the GPPs at the basin scale, with 0.83 for TRMM 3B42, 0.79 for GSMaP, 0.77 for CMORPH, and 0.76 for CPC. In terms of the five statistical indicators (Table 4), TRMM 3B42 had the best performance at the monthly scale, but with a slightly overestimated precipitation value, and CMORPH, CPC, and GSMaP had large errors with all indicators underestimating the precipitation.

**Table 4.** Average indexes of the rain gauge observations and precipitation products, at both the daily and the monthly time scales.

Time Scale	Precipitation Products	Mean (mm)	SE (mm)	RMSD (mm)	MAE (mm)	CC	PBIAS (%)	POD	FAR	CSI
Daily	Gauge	4.61	0.21	-	-	-	-	-	-	-
	CMORPH	3.73	0.15	11.75	4.87	0.40	-16	0.82	0.29	0.50
	CPC	3.65	0.14	11.44	4.83	0.40	-15	0.91	0.41	0.48
	GSMaP	3.52	0.13	10.73	4.56	0.44	-12	0.92	0.44	0.46
	TRMM 3B42	4.69	0.18	12.19	5.24	0.42	4	0.81	0.28	0.50
Monthly	Gauge	140.33	2.62	-	-	-	-	-	-	-
	CMORPH	113.60	1.82	97.05	65.09	0.77	-16	-	-	-
	CPC	110.96	1.85	99.58	68.20	0.76	-15	-	-	-
	GSMaP	104.63	1.79	91.71	63.70	0.79	-12	-	-	-
	TRMM 3B42	142.57	2.33	82.93	53.59	0.83	4	-	-	-

At the pixel scale, the spatial distributions of the indicators (CC, RMSD, and PBIAS) at a monthly scale over the study area are shown in Figure 3a–l). From the simulated data, it can be seen that TRMM 3B42 has the best CC values for the whole basin. The CC values of CPC and GSMaP are worst in the south-east region, ranging from 0.2 to 0.4, while those of CMORPH are relatively low in the upstream and south-west regions of the basin, in the range of 0.4–0.6 (Figure 3a–d).



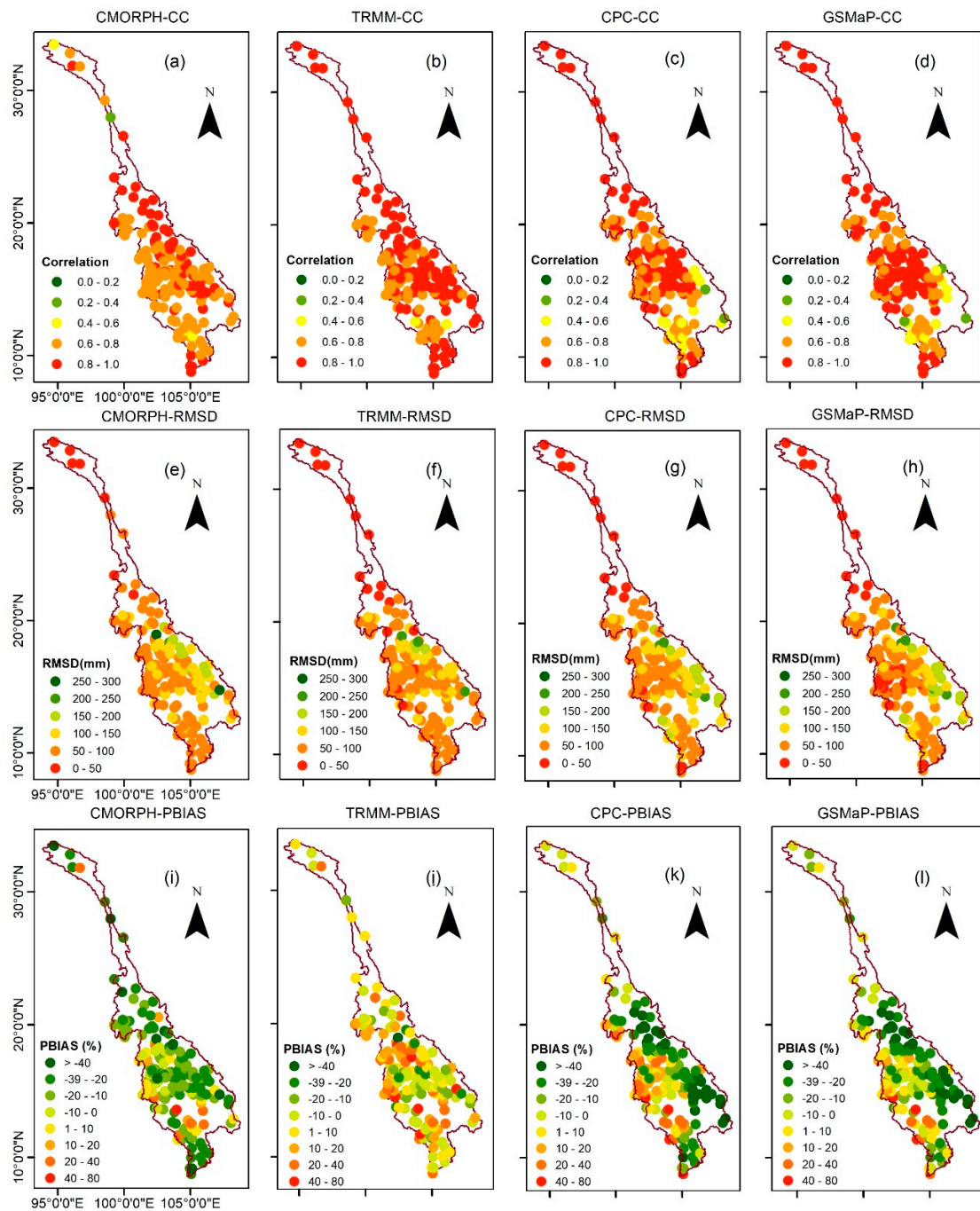


**Figure 3.** Spatial distributions of the correlation coefficient (CC) (a–d), the root-mean-squared deviation (RMSD) (mm/month) (e–h), and the percentage bias (PBIAS) (%) (i–l) between the GPPs and the gauge observations at the monthly scale during 1998–2006.

The RMSD shows a similar pattern, but to a different extent in all of the GPPs (Figure 3e–h). The RMSD of TRMM 3B42 is the lowest error (around 50–100 mm/month) at the monthly scale, compared to all of the other GPPs (250–300 mm/month). Very high RMSD values are seen in CPC and GSMaP in the south-east of the river basin, as shown in the Figure 3e–h, which is probably because this area is a high rainfall zone in the river basin. At the basin scale, TRMM 3B42 also has the smallest RMSD value (82.93 mm/month), while the RMSD values of GSMaP, CMORPH, and CPC are 91.71, 97.05, and 99.58 mm/month, respectively.

The distribution of PBIAS indicates that TRMM 3B42 performs the best compared to the others, since PBIAS shows the lowest values at both the grid scale, around 10% (Figure 3i–l), and the watershed scale, at 4% (Table 4). Considering CPC and GSMaP, their PBIAS values are consistently the worst in the east of basin—40% underestimation was seen—but the indicators are improved in the south-west of the basin, with PBIAS values of around 10% overestimation. In contrast, the PBIAS of CMORPH has no clear relationship with the gauge observations, sometimes overestimating or underestimating the observation by 20%–40%, as seen in Figure 3i–l. As expected, at the watershed scale, the PBIAS of GSMaP (−12%) and of CPC (−15%) can be considered to perform comparably better than CMORPH (−16%).

With monthly time series, it can be concluded that first, the TRMM 3B42 has the best performance at the basin scale, and CMORPH has the largest errors. Second, conducting analyses at the pixel scale further confirms the outperformance of the other models by TRMM 3B42, which is characterized by stable performance with observations in all of the indicators. In contrast, GSMaP, CPC, and CMORPH show inferior performances, especially in the south-east part of the basin.

#### 4.1.3. Daily Comparison

As shown in Table 4, in terms of the daily average precipitation, TRMM 3B42 has the smallest average errors (0.08 mm/day overestimation), while GSMaP has the largest (3.52 mm/day by GSMaP compared with 4.61 mm/day by observation). Similarly, TRMM 3B42 overestimates precipitation overall, with a PBIAS value of 4%, showing the best performance, while CMORPH, CPC, and GSMaP underestimate precipitation, with a PBIAS value of −16%, −15%, and −12%, respectively. With RMSD and MAE, the TRMM product performs worst, with large overestimations for RMSD of 12.19 mm/day and MAE of 5.24 mm/day; the other products—CMORPH, CPC, and GSMaP—performed slightly better, with both RMSD and MAE being 11.75–4.87, 11.44–4.83, and 10.73–4.56, respectively. Overall, higher accuracy can be seen more at the monthly scale than at the daily scale, a possible reason for which being that the errors at the daily scale are canceled out due to aggregation. The SE value for TRMM rainfall is 0.18 mm, which is closest to the ground observation, while those for GSMaP, CPC, and CMORPH rainfall, are 0.13, 0.14, 0.15, respectively.

Figure 4 plots the correlation coefficients between the GPPs and the rain observations, considering the effects of latitude. It can be seen that, in the upstream part of the basin (higher than 20° N latitude), the CC of GSMaP is highest compared to the other GPPs, and the CPC product has better correlation than CMORPH and TRMM. In the low- and mid-latitude regions (lower than 20° N latitude), the CC of GSMaP shows strong variation, reaching 0.9 at several stations—and even lower than 0.1 at some stations. A narrower variation in the range of [0.2,0.6] is presented in the CC of TRMM 3B42 and CMORPH. At the basin scale, the CCs of all of the selected GPPs are around 0.4; the GSMaP has the best overall performance with a CC of 0.44, while the CC of TRMM, CMORPH, and CPC is 0.42, 0.40, and 0.40, respectively. This result indicates that “calibration with rain gauge data” has the potential to improve the daily precipitation distribution for hydrometeorological applications, and the performance of GPPs, especially GSMaP, is strongly related to latitude.

The POD and CSI indicators were employed to analyze the ability to detect precipitation of all of the selected GPPs, and 0.1 mm/day was defined as the threshold of rain/no-rain detection [39]. Generally, the POD of all of the GPPs shows a good value, larger than 0.81 (Table 4); the POD of GSMaP and CPC is observed to be larger than 0.91, with an insignificant FAR of 0.44 for GSMaP and 0.41 for CPC, which indicates that the GSMaP and CPC data generally have more rain days compared to the observations. The CSI indicators of TRMM and CMORPH (0.5) are higher than those of GSMaP and CPC (0.46–0.48), which indicates that TRMM and CMORPH better detect precipitation than GSMaP and CPC.

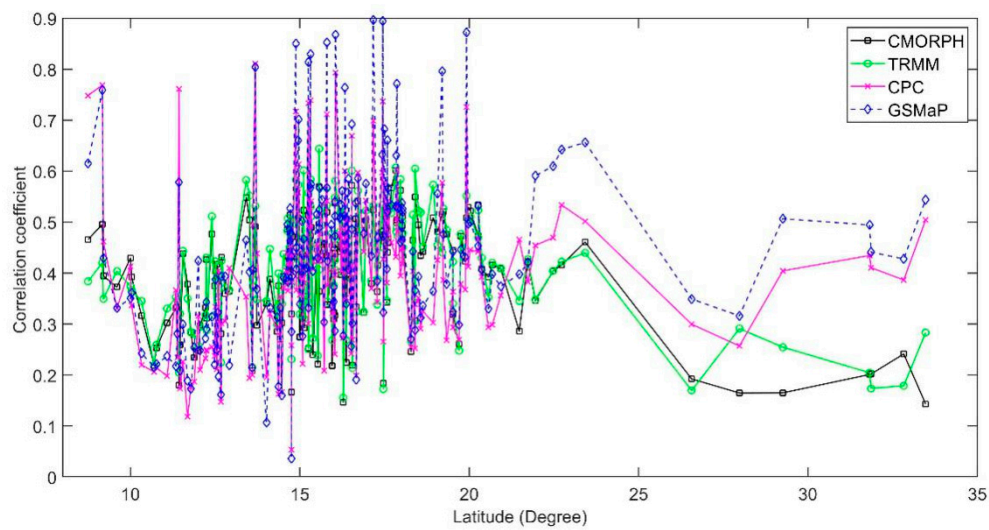


**Figure 4.** Correlation coefficients of the GPPs and the observed rainfall with latitude.

Figure 5 shows the frequency of rainfall events (bar chart) and their relative contributions to the total accumulative rainfall from the 1998–2006 period (line chart) by different rainfall classification of the four GPPs and rain gauge observations at the daily scale. Overall, the GPPs underestimate rainfall frequency, as well as the contributions of no rain (rain  $\leq 0.1$  mm) and moderate/heavy rain events (rain  $> 20$  mm) compared to the observations. Conversely, with the little and light rain intensities ( $0.1 < \text{rain} \leq 20$  mm), both the occurrence frequencies and their contributions of the gridded data are overestimated in comparison to the rain gauges. The contribution of light rain shows the highest contribution in the GPPs, while the highest contribution of observation is from the moderate (20,50] mm rainfall class.

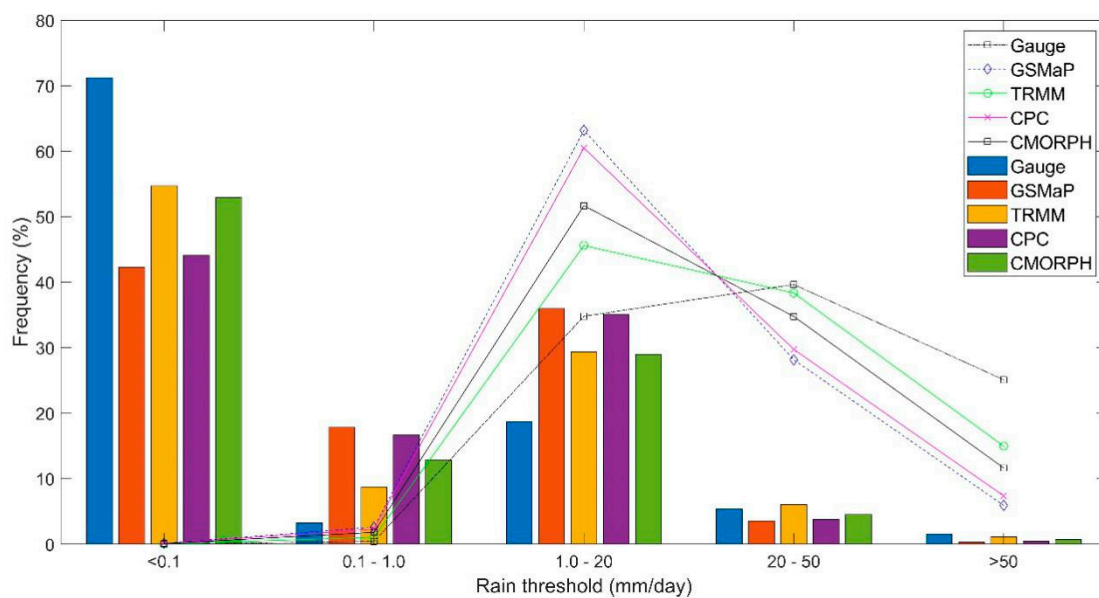


**Figure 5.** The occurrence frequencies (bars) of CPC, TRMM 3B42, GSMaP, CMORPH, and the daily gauge observations, as well as their relative contributions (lines) to the total rainfall during the period 1998–2006.

GSMaP shows the largest discrepancy with the observations, both in frequency and contribution, in all rain intensity classes. The frequency is 27% higher than that of the observations in the little rain class (0.1,1) mm—31.3% for GSMaP and 4.3% for the observations. The rainfall of all of the GPPs in

this class provides an insignificant contribution. At the light rain intensity (1,20] mm, the occurrence frequency of GSMaP is 36.3% compared to 20.7% for the observations, and the contribution is 62.5% and 35% for GSMaP and the observations, respectively, which is nearly a 30% difference. The CPC and CMORPH products illustrate the same variation, but with a narrower spread compared to GSMaP—the occurrence frequency of 27% and 20% with little rain, and 35.5% and 28.7% with moderate rain, respectively.

TRMM 3B42 deviates the least compared to the observations regarding the occurrence frequencies and contributions of all rainfall intensities, as shown in Figure 5. TRMM 3B42 estimates the occurrence frequency of little rain events to be approximately 11.7%, which is approximately 7% lower than the actual occurrence frequency. TRMM 3B42 estimates the occurrence frequency of light rainfall events to be approximately 29.14%, which is approximately 8% higher than the actual occurrence frequency, and the contribution to be 45%, which is 15% higher than the observations. With moderate rain class (20,50] mm, the contribution of TRMM 3B42 even matches that of the observations—38% and 39%, respectively. At heavy intensity (>50 mm), the difference between TRMM and the observations, both in occurrence frequency and contribution, is also lowest—0.62% and 10%, respectively.

In other words, quantitatively analyzing the discrepancies between the GPPs and the rain gauge data in terms of the rain class first shows that all of the GPPs feature similar error characteristics, i.e., they tend to overestimate little and light rainfall events, but underestimate moderate and heavy ones. Significant discrepancies can be found in the GSMaP product in contrast to the narrowest spread presented in TRMM 3B42. Second, all of the GPPs perform poorly in capturing heavy rainfall (>50 mm/day) events, which suggests that local calibration with rain gauge or ground radar data should be carried out to further improve the daily precipitation estimates for further studies.

The analysis of statistical indicators proves that the TRMM 3B42 product illustrates the best ability to capture precipitation for the whole MRB at different time scales: Monthly, seasonal, and annual comparisons. It can be found that at the daily time scale, the GSMaP and CPC products show better performance than the other GPPs in the upstream region of the basin.

Evaluation of the different GPPs at different variability scales (i.e., spatial and temporal scales) using statistical indicators provides an overall picture of the GPPs' performance. To enable the guiding of users to more precisely select the appropriate product for hydrological applications, multiple GPPs should be tested in hydrological simulations [48,49]. Therefore, in this study, further simulations of the daily hydrological process in the MRB using the SWAT model were conducted.

#### 4.2. Evaluation of Precipitation Products' Hydrological Performance using SWAT Model

This section explores the potential of the selected precipitation products for hydrological simulation over the MRB using the SWAT model. The model was calibrated against the daily discharge collected from six hydrological gauges within the MRB. Sensitive analysis and model calibration were performed using the SUFI-2 algorithm integrated into the SWAT-CUP tool. The analysis was conducted over 8 years (1998–2006) with different precipitation data at daily time scales, while the other meteorological information remained unchanged.

##### 4.2.1. Evaluation of Model Performance

The 1998 data were used as a “warm-up” period to initialize the model, and the data from the rain gauge observations and the three GPPs (CPC, TRMM 3B42, and CMORPH) from 1999 to 2006 were used for model calibration. With GSMaP, the precipitation from 2001 to 2006 was used for model calibration, with the 2000 dataset used for the warm-up period, due to a lack of obtained data. This calibration procedure was performed at each individual discharge gauge and for each individual GPP. The best model parameter values obtained for each precipitation product for the calibration period are presented in Figure 6 and Table 5.



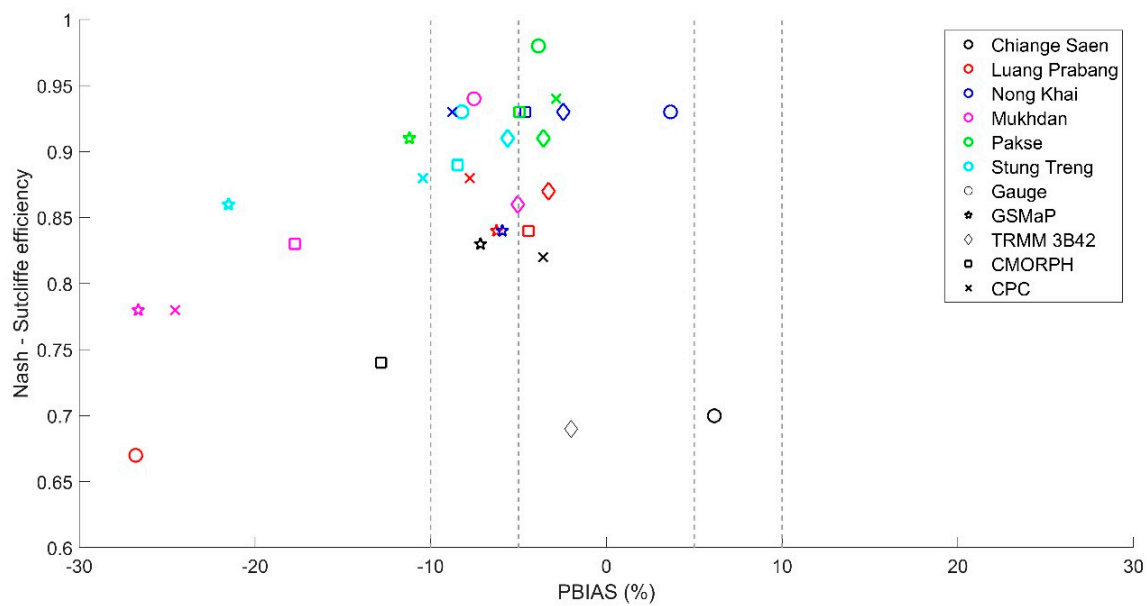


**Figure 6.** Nash–Sutcliffe efficiency coefficient (NSE) and PBIAS of values of the hydrological stations.

**Table 5.** Statistics index for the models of the Mekong River Basin using SWAT at six different stations.

Station	Statistics Index	Gauge	GSMaP	TRMM 3B42	CMORPH	CPC
Chiange Saen	NSE	0.7	0.83	0.69	0.74	0.82
	PBIAS	6.14	−7.16	−2.01	−12.81	−3.61
	R <sup>2</sup>	0.81	0.86	0.79	0.77	0.85
Luang Prabang	NSE	0.67	0.84	0.87	0.84	0.88
	PBIAS	−26.78	−6.25	−3.29	−4.43	−7.78
	R <sup>2</sup>	0.88	0.94	0.95	0.94	0.98
Nong Khai	NSE	0.93	0.84	0.93	0.93	0.93
	PBIAS	3.65	−5.93	−2.45	−4.62	−8.76
	R <sup>2</sup>	0.97	0.94	0.97	0.95	0.96
Mukhdan	NSE	0.94	0.78	0.86	0.83	0.78
	PBIAS	−7.54	−26.64	−5.04	−17.73	−24.54
	R <sup>2</sup>	0.98	0.93	0.96	0.95	0.94
Pakse	NSE	0.98	0.91	0.91	0.93	0.94
	PBIAS	−3.87	−11.21	−3.58	−4.95	−4.86
	R <sup>2</sup>	0.98	0.97	0.97	0.98	0.98
Stung Treng	NSE	0.93	0.86	0.91	0.89	0.88
	PBIAS	−8.23	−21.51	−5.62	−8.47	−10.44
	R <sup>2</sup>	0.98	0.97	0.99	0.97	0.97

The P-factor and R-factor results for the calibration range from 0.68–0.98 and 0.67–1.55, respectively, which reveals that all of the simulations to capture streamflow discharge acquire reasonable uncertainties [45]. The simulated streamflow reproduced by the different GPPs at each individual station is satisfactory, with NSE > 0.67 and R<sup>2</sup> > 0.77 (Table 5).

The models using the GSMaP and CPC products as the precipitation data attain excellent performance for the upstream part of the MRB during the calibration period, with NSE and R<sup>2</sup> at Chiange Saen and Luang Prabang being in the range of 0.82 and 0.86, respectively (Figure 6), while the performances with the observation data for the calibration periods are 0.7 for NSE and 0.81 for R<sup>2</sup>. These results indicate that the spatial coverage of the rainfall stations in the upstream part of the MRB does not feature a sufficient density to reflect the rainfall characteristics in this region. Calibrating the SWAT model with individual gridded precipitation further improves streamflow simulations



compared to the model calibrated with gauges for the sparse-rain gauge region in the upstream part of the MRB. Although individual precipitation may possess large biases, calibration may mitigate the errors of such biases. Over the northern section of the river basin with sparse gauges, the use of GPPs is more reasonable than that of gauge-based precipitation products.

At Nong Khai station (mid-latitude region), the fitting of the simulated streamflow of the GSMaP data-forced model has relatively lower but still reasonable performance compared to the other precipitation products, with an NSE and  $R^2$  of around 0.84 and 0.94, while those same values for CPC, Gauge, CMORPH, and TRMM 3B42 are around 0.93 and 0.97, respectively. In addition, the PBIAS values in this area vary from 3.65 to  $-8.76$  for all of the GPPs' forced simulations, showing a large variability in the performances between the different GPPs.

At the Mukhdan, Pakse, and Stung Treng gauges (i.e., the eastern part), the best performance is attained when using the rain gauge observation data, with the NSE being around 0.94 and the  $R^2$  being 0.98 for all three of the stations. This is simply because the highest density of rainfall is collected, which better reflects the precipitation characteristics for this sub-region (Figure 6). All of the GPPs' forced data simulations exhibit satisfactory performance, with the NSE changing from 0.78 to 0.89. The lowest NSE can be seen for GSMaP.

The TRMM 3B42 forced simulation exhibits an almost negligible PBIAS ( $-5.62\%$  to  $-2.01\%$ ), suggesting its promising potential to replace in situ observations in hydrologic applications, even though it produces a slightly lower streamflow than that of the observations. The simulation of GSMaP shows large variation of the PBIAS (from  $-26.64\%$  to  $-5.93\%$ ), which suffers from serious underestimation, especially in the eastern part of the basin (Table 5). A similar tendency as that of GSMaP is visualized during the simulation of CPC, with the highest PBIAS at the Mukhdan and Stung Treng gauges being  $-24.54\%$  and  $-10.44\%$ , respectively.

Overall, at the daily scale, there is a large variability in hydrological performance depending on the GPP being used. In the upstream part of the basin, CPC attains the best performance, while in the mid- and low-latitude regions, the best performance can be seen by TRMM 3B42's forced simulations.

#### 4.2.2. Water Balance Components at the Sub-Region Scale

As mentioned above, the application of a GPP is specific to the location. This uncertainty in precipitation will propagate into water balance components. Therefore, for water balance analysis, the Mekong mainstream river was divided into six regions, respectively, with six hydrological stations (Figure 7).

Region 1 (R1): Lancang Jiang or Upper Mekong River in China, limited by Chiange Saen gauge;

Region 2a (R2a): Chiang Saen to Luang Prabang (Upper Nam Ou in Lao PDR);

Region 2b (R2b): Luang Prabang to Nong Khai (northeast Lao PDR);

Region 2c (R2c): Nong Khai to Mukdahan (central Lao PDR, which includes the Nam SongKharam and Nam Cadinh tributary systems);

Region 3 (R3): Mukdahan to Pakse (south Lao PDR and Korat Plateau, which includes the Mun and Chi tributary systems);

Region 4 (R4): Pakse to Stungtreng (Se Kong, Se San and Sre Pok and in Cambodia, Vietnam);

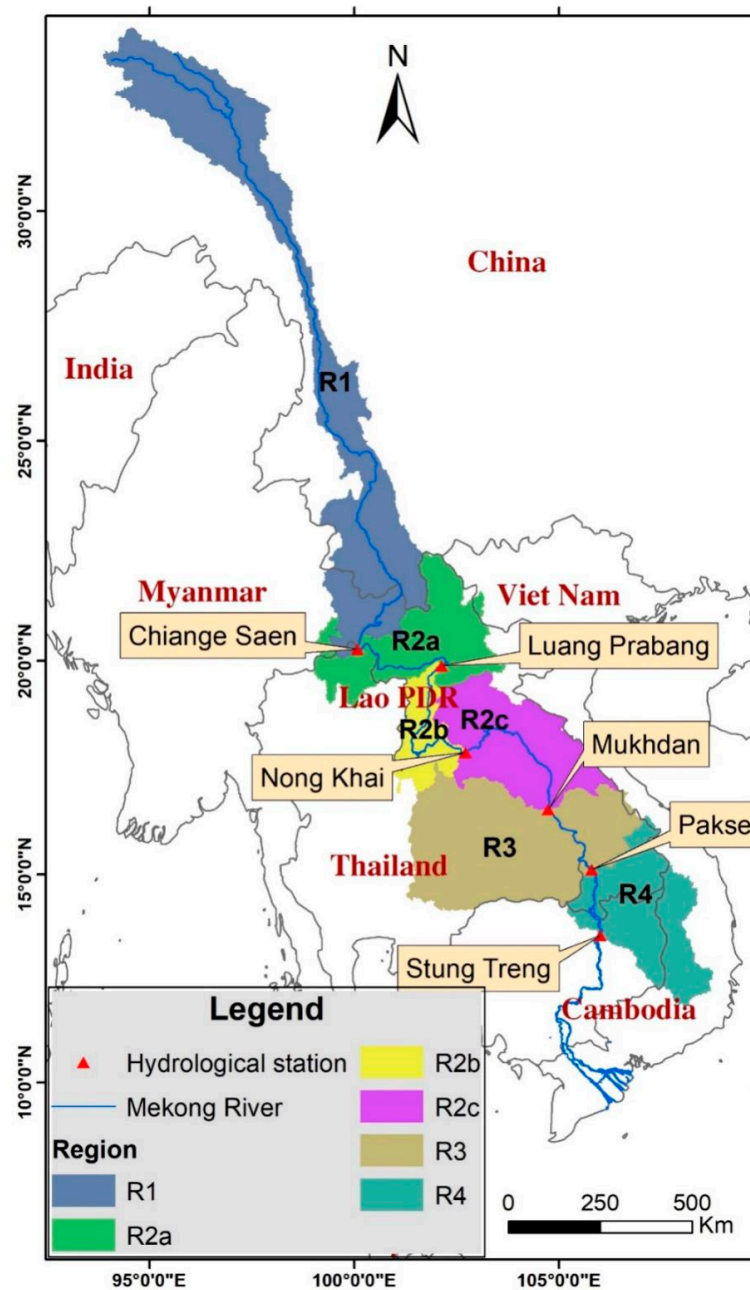


**Figure 7.** Sub-regions for the water balance analysis in the Mekong River Basin.

Figure 8 shows the variability of precipitation (P), evapotranspiration (ET), groundwater recharge (GW), and runoff (R) for each GPP obtained from SWAT model simulations for sub-regions in the MRB. A significant variation of all water-balance components under different GPPs is observed for each sub-region. These uncertainties are also expressed with a wide range of standard errors (SE), as presented in Table 6. The variation of precipitation could be the main reason for the variations of other water-balance components. In the R1 sub-region, for example, the variation of P among GPPs is much smaller than those in other sub-regions, and similar variations are found for other water-balance components. As a result, the selection of relevant GPPs for a specific sub-region is important for the reliability of water-balance components and water-resource evaluation. Based on the PBIAS and NSE values, it is recommended that CPC products be used for R1, TRMM for R2a, R2b, R2c, R4, and gauge products for R3. The quantitative analysis of the water-balance components using the recommended rainfalls as inputs for respective sub-regions is displayed in Table 6.

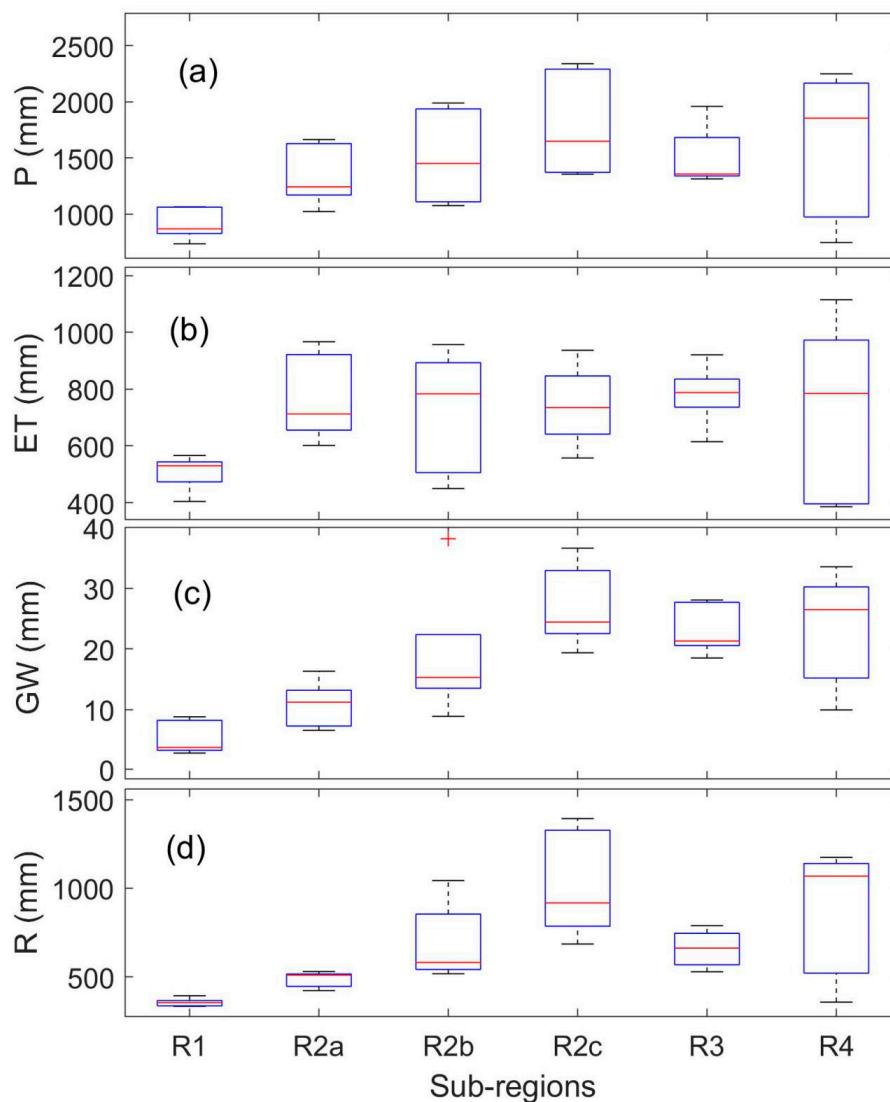


**Figure 8.** (a) Precipitation (P), (b) evapotranspiration (ET), (c) groundwater recharge (GW) and (d) total runoff (R) of the sub-regions obtained from SWAT model simulations for each of the GPPs. Box plots display the 25th, 50th, and 75th percentiles.

**Table 6.** Water balance components of the sub-regions in the Mekong River Basin.

Components/Region	R1	R2a	R2b	R2c	R3	R4
Precipitation (mm)	857	1615	1988	2338	1958	2247.9
SE (mm)	63.7	123.5	192.4	214.0	121.7	300.5
Evaporation and transpiration (mm)	496.3	967.0	956.9	936.9	921.0	1114.9
(% compared with rainfall)	(58%)	(60%)	(48%)	(40%)	(47%)	(50%)
SE (mm)	27.9	70.1	98.6	64.4	49.0	144.4
Total runoff depth (mm)	357.3	511.0	1043.6	1305.7	662.2	1174.5
(% compared with rainfall)	(42%)	(32%)	(53%)	(56%)	(34%)	(52%)
SE (mm)	10.6	20.2	99.1	138.5	47.5	165.5
Surface runoff	14.3	5.1	73.1	195.9	390.7	129.19
Baseflow	343.0	505.9	970.5	1109.9	271.5	1045.3
Groundwater recharge	3.7	12.1	17.1	31.7	21.2	33.52
(% compared with rainfall)	(0.44%)	(0.75%)	(0.86%)	(1.35%)	(1.10%)	(1.50%)
SE (mm)	1.3	1.7	5.0	3.1	1.9	4.3

Precipitation over the basin is highly variable, ranging from 2338 mm in R2c to 857 mm in R1 (Upper Mekong River in China). The highest rainfall regions, R2c and R4, generally correspond to the areas of high elevation along the Annamite Range and are covered primarily by forest (around 60%) with a streamflow–precipitation ratio of approximately 0.6. The distribution of total runoff depth in the MRB closely reflects the spatial patterns in rainfall, with much higher proportions of rainfall (approximately 60%) translated into streamflow in R2c and R4, and with the greatest runoff of up to 1305.7 in R2c as the annual average for the 7-year period.

The precipitation in R2a, R2b, and R3 is lower than that in R2c and R4, but is still relatively high—from 1615 mm in R2a to approximately 2000 mm in R2b and R3. This R2a and R2b area is almost entirely mountainous and is covered with natural forest (nearly 90% in R2a and around 60% in R2b). These areas have high evapotranspiration and low surface runoff due to the high subsurface flow. Since R2a is still dominated by characteristics of R1, the evapotranspiration in R2a occupies up to 60%, and the surface runoff occupies only 4% in the total runoff depth. Additionally, R2b has a wide scope for agriculture (30% of the area), therefore much higher proportions of rainfall are translated into streamflow compared with R2a (up to 53%). Agriculture dominates in R3 and is reported to account for more than 80% of the area [32,33]. Consequently, the surface runoff is high, accounting for approximately 60% of the total flow. This region also has a high evaporation rate, accounting for 47%.

The rainfall in R1 decreases as the altitude increases toward the north; in this region, the mean rainfall is only 857 mm, and evapotranspiration is around 60%. Land use in this region is mainly divided into two major components: The majority is covered primarily by grassland (50%), while a further 40% is covered primarily by forest. This region has a very low runoff coefficient, but the streamflow–precipitation ratio accounts for up 42% of the total rainfall due to the major source of water flowing into the river coming from the melting snow on the Tibetan Plateau.

## 5. Conclusions

In this study, we analyzed four GPPs (TRMM 3B42, CMORPH, GSMaP, and CPC) and their hydrological application over the whole MRB for a nine-year period (1998–2006). We applied statistical indicators to evaluate the consistency between GPPs and the precipitation observations, and applied the SWAT model for analysis of the water balance components. The following major findings are concluded:

1. Considering the statistical indicators and the average precipitation, TRMM 3B42 illustrated the best ability to capture precipitation at the annual, seasonal, and monthly scales. At the daily scale, GSMaP and CPC showed a better performance and should be considered for use, especially for the upstream region of the basin.
2. With each dataset calibrated individually by the SWAT model, satisfactory performances were achieved at the daily scale for all of the GPPs and the gauge-driven models. For the ungauged or sparsely gauged regions, better performance was seen from the GPPs than the gauge-driven models, especially for the CPC product. In the downstream regions, TRMM showed the best performance, except for the gauge-driven models. These results further confirm the appropriateness of the GPPs at the daily time scale, which suggests its promising potential to replace in situ observations in hydrologic applications and its potential in the performance of all water balance components.
3. This study attempted to use different GPPs for each individual sub-region to evaluate the water balance components, suggesting strong capabilities for utilizing the advantages of publicly available GPPs in hydrological applications.
4. The spatial variability of water balance components was analyzed in the sub-regions. The distribution of total runoff depth is consistent with the spatial patterns in rainfall, but the landscape, soil texture, and terrain are also major factors that shape the distribution of streamflow. Forests are the major water yield for vegetation types, contributing to the baseflow, while agriculture offers factor-driven high surface runoff.

Generally, TRMM 3B42 is more robust than the other GPPs and is a reliable data source for hydrological applications in data-sparse area. The spatial variability of the water balance components should be analyzed based on the simulation with distinct suggested GPPs for each of the different sub-regions, which provides better references for the assessment and management of the basin water resources in data-scarce regions. Our findings are useful for selecting which GPP is suitable for advanced hydrological applications for each sub-region. Further studies should examine statistical distribution analysis and include extreme precipitation and the possible prediction of rainfall products over the river basin in order to add more inference and generalization to this study.

**Author Contributions:** This manuscript is a result of the research of K.D.D. under the supervision of T.N.A. and the advice of D.D.B., N.Y.N. and R.S. This paper was finished under the efforts of all authors. All authors have read and agreed to the published version of the manuscript.

**Funding:** This research was funded by the Ministry of Science and Technology of Vietnam with the project code: NĐT.58.RU/19, and Vingroup Innovation Foundation with the project code: VINIF.2019.DA17.

**Acknowledgments:** We are grateful to the providers of operational satellite precipitation products and rain gauge measurements for making data available to us. We would also like to extend our acknowledgements to the editors and anonymous reviewers for their valuable comments and advice.

**Conflicts of Interest:** The authors declare no conflicts of interest

## References

1. Senent-Aparicio, J.; López-Ballesteros, A.; Pérez-Sánchez, J.; Segura-Méndez, F.J.; Pulido-Velazquez, D. Using Multiple Monthly Water Balance Models to Evaluate Gridded Precipitation Products over Peninsular Spain. *Remote Sens.* **2018**, *10*, 922. [[CrossRef](#)]
2. Wu, Z.; Xu, Z.; Wang, F.; He, H.; Zhou, J.; Wu, X.; Liu, Z. Hydrologic evaluation of Multi-Source satellite precipitation products for the Upper Huaihe River Basin, China. *Remote Sens.* **2018**, *10*, 840. [[CrossRef](#)]
3. Mcmillan, H.; Jackson, B.; Clark, M.; Kavetski, D.; Woods, R. Rainfall uncertainty in hydrological modelling: An evaluation of multiplicative error models. *J. Hydrol.* **2011**, *400*, 83–94. [[CrossRef](#)]
4. Arkin, A.; Xie, P. A 17-year monthly analysis based on gauge observations, satellite estimates, and numerical model outputs. *Bull. Am. Meteorol. Soc.* **1997**, *78*, 2539–2558.
5. Huffman, G.J.; Adler, R.F.; Morrissey, M.M.; Bolvin, D.T.; Curtis, S.; Joyce, R.; McGavock, B.; Susskind, J. Global Precipitation at One-Degree Daily Resolution from Multisatellite Observations. *J. Hydrometeorol.* **2001**, *2*, 36–50. [[CrossRef](#)]
6. Mishra, A.K.; Coulibaly, P. Developments in hydrometric network design: A review. *Dtsch. Welle* **2013**, 1–24. [[CrossRef](#)]
7. Zhang, C.; Chen, X.; Shao, H.; Chen, S.; Liu, T.; Chen, C.; Ding, Q.; Du, H. Evaluation and intercomparison of high-resolution satellite precipitation estimates-GPM, TRMM, and CMORPH in the Tianshan Mountain Area. *Remote Sens.* **2018**, *10*, 1543. [[CrossRef](#)]
8. Tian, Y.; Peters-Lidard, D.C.; Adler, R.F.; Kubota, T.; Ushio, T. Evaluation of GSMaP Precipitation Estimates over the Contiguous United States. *J. Hydrometeorol.* **2010**, *11*, 566–574. [[CrossRef](#)]
9. Zhang, J.; Howard, K.; Langston, C.; Vasiloff, S.; Kaney, B.; Arthur, A.; Van Cooten, S.; Kelleher, K.; Kitzmiller, D.; Ding, F.; et al. National mosaic and multi-sensor QPE (NMQ) system description, results, and future plans. *Bull. Am. Meteorol. Soc.* **2011**, *92*, 1321–1338. [[CrossRef](#)]
10. Anagnostou, M.N.; Nikolopoulos, E.I.; Kalogiros, J.; Anagnostou, E.N.; Marra, F.; Mair, E.; Bertoldi, G.; Tappeiner, U.; Borga, M. Advancing precipitation estimation and streamflow simulations in complex terrain with X-Band dual-polarization radar observations. *Remote Sens.* **2018**, *10*, 1258. [[CrossRef](#)]
11. Xue, X.; Hong, Y.; Limaye, A.S.; Gourley, J.J.; Huffman, G.J.; Khan, S.I.; Dorji, C.; Chen, S. Statistical and hydrological evaluation of TRMM-based Multi-satellite Precipitation Analysis over the Wangchu Basin of Bhutan: Are the latest satellite precipitation products 3B42V7 ready for use in ungauged basins? *J. Hydrol.* **2013**, *499*, 91–99. [[CrossRef](#)]
12. Ebert, E.E.; Janowiak, J.E.; Kidd, C. Comparison of near-real-time precipitation estimates from satellite observations and numerical models. *Bull. Am. Meteorol. Soc.* **2007**, *88*, 47–64. [[CrossRef](#)]



13. Guo, H.; Chen, S.; Bao, A.; Hu, J.; Gebregiorgis, A.S.; Xue, X.; Zhang, X. Inter-comparison of high-resolution satellite precipitation products over Central Asia. *Remote Sens.* **2015**, *7*, 7181–7211. [[CrossRef](#)]
14. Gebremichael, M.; Menberu, M.B.; Feyera, A.H.; Tesfay, G.N. Accuracy of satellite rainfall estimates in the Blue Nile Basin: Lowland plain versus highland mountain. *Water Resour. Res. AGU Publ.* **2014**, 8775–8790. [[CrossRef](#)]
15. Sorooshian, S.; Aghakouchak, A.; Arkin, P.; Eylander, J.; Fofoula-Georgiou, E.; Harmon, R.; Hendrickx, J.M.H.; Imam, B.; Kuligowski, R.; Skahill, B.; et al. Advanced concepts on remote sensing of precipitation at multiple scales. *Bull. Am. Meteorol. Soc.* **2011**, *92*, 1353–1357. [[CrossRef](#)]
16. Tuo, Y.; Duan, Z.; Disse, M.; Chiogna, G. Evaluation of precipitation input for SWAT modeling in Alpine catchment: A case study in the Adige river basin (Italy). *Sci. Total Environ.* **2016**, *573*, 66–82. [[CrossRef](#)]
17. Chen, A.; Chen, D.; Azorin-Molina, C. Assessing reliability of precipitation data over the Mekong River Basin: A comparison of ground-based, satellite, and reanalysis datasets. *Int. J. Climatol.* **2018**, *38*, 4314–4334. [[CrossRef](#)]
18. Tobin, K.J.; Bennett, M.E. Using SWAT to Model Streamflow in Two River Basins With Ground and Satellite Precipitation Data. *JAWRA J. Am. Water Resour. Assoc.* **2009**, *45*, 253–271. [[CrossRef](#)]
19. Arnold, J.G.; Moriasi, D.N.; Gassman, P.W.; Abbaspour, K.C.; White, M.J.; Srinivasan, R.; Santhi, C.; Harmel, R.D.; van Griensven, A.; Van Liew, M.W.; et al. SWAT: Model Use, Calibration, and Validation. *Trans. ASABE* **2012**, *55*, 1317–1335. [[CrossRef](#)]
20. Devia, G.K.; Ganasri, B.P.; Dwarakish, G.S. A Review on Hydrological Models. *Aquat. Procedia* **2015**, *4*, 1001–1007. [[CrossRef](#)]
21. Michaelides, S.; Levizzani, V.; Anagnostou, E.; Bauer, P.; Kasparis, T.; Lane, J.E. Precipitation: Measurement, remote sensing, climatology and modeling. *Atmos. Res.* **2009**, *94*, 512–533. [[CrossRef](#)]
22. Jiang, D.; Wang, K. The role of satellite-based remote sensing in improving simulated streamflow: A review. *Water (Switzerland)* **2019**, *11*, 1615. [[CrossRef](#)]
23. Chen, M.; Xie, P. CPC Unified Gauge-based Analysis of Global Daily Precipitation. Available online: <https://climatedataguide.ucar.edu/climate-data/cpc-unified-gauge-based-analysis-global-daily-precipitation> (accessed on 1 June 2020).
24. Huffman, G.J.; Bolvin, D.T. TRMM and Other Data Precipitation Data Set Documentation. Available online: [https://gpm.nasa.gov/sites/default/files/document\\_files/3B42\\_3B43\\_doc\\_V7.pdf](https://gpm.nasa.gov/sites/default/files/document_files/3B42_3B43_doc_V7.pdf) (accessed on 1 June 2020).
25. Joyce, R.J.; Janowiak, J.E.; Arkin, P.A.; Xie, P. CMORPH: A Method that Produces Global Precipitation Estimates from Passive Microwave and Infrared Data at High Spatial and Temporal Resolution. *J. Hydrol. Reg. Stud.* **2004**. [[CrossRef](#)]
26. Kubota, T.; Hashizume, H.; Shige, S.; Okamoto, K.; Aonashi, K.; Takahashi, N.; Ushio, T.; Kachi, M. Global precipitation map using satelliteborne microwave radiometers by the GSMaP project: Production and validation. *Int. Geosci. Remote Sens. Symp.* **2006**, *45*, 2584–2587.
27. Mohammed, I.N.; Bolten, J.D.; Srinivasan, R.; Lakshmi, V. Improved hydrological decision support system for the Lower Mekong River Basin using satellite-based earth observations. *Remote Sens.* **2018**, *10*, 885. [[CrossRef](#)] [[PubMed](#)]
28. Wang, W.; Lu, H.; Yang, D.; Sothea, K.; Jiao, Y.; Gao, B.; Peng, X.; Pang, Z. Modelling hydrologic processes in the Mekong River basin using a distributed model driven by satellite precipitation and rain gauge observations. *PLoS ONE* **2016**, *11*, 1–19. [[CrossRef](#)]
29. Lauri, H.; De Moel, H.; Ward, P.J.; Räsänen, T.A.; Keskinen, M.; Kummu, M. Future changes in Mekong River hydrology: Impact of climate change and reservoir operation on discharge. *Hydrol. Earth Syst. Sci.* **2012**, *16*, 4603–4619. [[CrossRef](#)]
30. Räsänen, T.A.; Someth, P.; Lauri, H.; Koponen, J.; Sarkkula, J.; Kummu, M. Observed river discharge changes due to hydropower operations in the Upper Mekong Basin. *J. Hydrol.* **2017**, *545*, 28–41. [[CrossRef](#)]
31. Bui, D.; Tran, D.M.; Vu, H.T.; Bui, N.T. Developing a Coupling Model System of Global Rainfall Data and Open-Source Model for Water Forecast in Poorly Gauged Basins. *J. Adv. Eng. Comput.* **2019**, *3*, 355. [[CrossRef](#)]
32. MRC. *State of the Basin Report 2010*; Taylor, R., Ed.; Lao PDR: Vientiane, Laos, 2010; ISBN 9789932080571.
33. MRC Data and Information Services. Available online: <https://portal.mrcmekong.org/> (accessed on 18 April 2020).

34. Mekong River Commission, Overview of the Hydrology of the Mekong Basin. Available online: <http://www.mekonginfo.org/assets/midocs/0001968-inland-waters-overview-of-the-hydrology-of-the-mekong-basin.pdf> (accessed on 1 June 2020).
35. Chen, M.; Shi, W.; Xie, P.; Silva, V.B.S.; Kousky, V.E.; Higgins, R.W.; Janowiak, J.E. Assessing objective techniques for gauge-based analyses of global daily precipitation. *J. Geophys. Res. Atmos.* **2008**, *113*, 1–13. [[CrossRef](#)]
36. Schneider, U.; Becker, A.; Finger, P.; Meyer-Christoffer, A.; Ziese, M.; Rudolf, B. GPCP's new land surface precipitation climatology based on quality-controlled in situ data and its role in quantifying the global water cycle. *Theor. Appl. Climatol.* **2014**, *115*, 15–40. [[CrossRef](#)]
37. HydroSHEDS. Available online: <https://www.hydrosheds.org/> (accessed on 18 April 2020).
38. Food and Agriculture Organization of the United Nations. Available online: <http://www.fao.org/soils-portal/soil-survey/soil-maps-and-databases/en/> (accessed on 18 April 2020).
39. Gosset, M.; Viarre, J.; Quantin, G.; Alcoba, M. Evaluation of several rainfall products used for hydrological applications over West Africa using two high-resolution gauge networks. *Q. J. R. Meteorol. Soc.* **2013**, *139*, 923–940. [[CrossRef](#)]
40. Ren, P.; Li, J.; Feng, P.; Guo, Y.; Ma, Q. Evaluation of multiple satellite precipitation products and their use in hydrological modelling over the Luanhe River Basin, China. *Water (Switzerland)* **2018**, *10*, 677. [[CrossRef](#)]
41. Tan, M.; Ibrahim, A.; Duan, Z.; Cracknell, A.; Chaplot, V. Evaluation of Six High-Resolution Satellite and Ground-Based Precipitation Products over Malaysia. *Remote Sens.* **2015**, *7*, 1504–1528. [[CrossRef](#)]
42. Li, Y.; Thompson, J.R.; Li, H. Impacts of spatial climatic representation on hydrological model calibration and prediction uncertainty: A mountainous catchment of Three Gorges Reservoir Region, China. *Water (Switzerland)* **2016**, *8*, 73. [[CrossRef](#)]
43. Ruan, H.; Zou, S.; Yang, D.; Wang, Y.; Yin, Z.; Lu, Z.; Li, F.; Xu, B. Runoff simulation by SWAT model using high-resolution gridded precipitation in the upper Heihe River Basin, Northeastern Tibetan Plateau. *Water (Switzerland)* **2017**, *9*. [[CrossRef](#)]
44. Tang, X.; Zhang, J.; Gao, C.; Ruben, G.; Wang, G. Assessing the Uncertainties of Four Precipitation Products for Swat Modeling in Mekong River Basin. *Remote Sens.* **2019**, *11*, 304. [[CrossRef](#)]
45. Thom, V.T.; Khoi, D.N.; Linh, D.Q. Using gridded rainfall products in simulating streamflow in a tropical catchment-A case study of the Srepok River Catchment, Vietnam. *J. Hydrol. Hydromech.* **2017**, *65*, 18–25. [[CrossRef](#)]
46. Abbaspour, K.C. SWAT-CUP: SWAT Calibration and Uncertainty Programs-A User Manual. Available online: [https://swat.tamu.edu/media/114860/usermanual\\_swatcup.pdf](https://swat.tamu.edu/media/114860/usermanual_swatcup.pdf) (accessed on 1 June 2020).
47. Nash, J.E.; Sutcliffe, J.V. River flow forecasting through conceptual models part I—A discussion of principles. *J. Hydrol.* **1970**, *10*, 282–290. [[CrossRef](#)]
48. Peng, B.; Shi, J.; Ni-Meister, W.; Zhao, T.; Ji, D. Evaluation of TRMM multisatellite precipitation analysis (tmpa) products and their potential hydrological application at an arid and semiarid basin in china. *IEEE J. Sel. Top. Appl. Earth Obs. Remote Sens.* **2014**, *7*, 3915–3930. [[CrossRef](#)]
49. Li, Z.; Yang, D.; Gao, B.; Jiao, Y.; Hong, Y.; Xu, T. Multiscale hydrologic applications of the latest satellite precipitation products in the Yangtze river basin using a distributed hydrologic model. *J. Hydrometeorol.* **2015**, *16*, 407–426. [[CrossRef](#)]

